

Stabilization of Z pinch by velocity shear

S. DeSouza-Machado,^{a)} A. B. Hassam, and Ramin Sina

Department of Physics, University of Maryland, College Park, Maryland 20742

(Received 18 April 2000; accepted 15 August 2000)

A numerical experiment is run to assess the stabilization of ideal magnetohydrodynamic (MHD) instabilities by externally applied velocity shear. A Z pinch, unstable to both kink and interchange (sausage) instabilities, is subjected to an external force that drives sheared mass flow along the axis. The turbulence from the MHD instabilities is found to be suppressed significantly with increasing Mach number of the flow. At sonic Mach numbers of 4–5, the “discharge” is seen to have recovered to its laminar state in more than 95% of the volume, there being a small residual wobble at the center of the column. For lower Mach numbers, the wobble becomes more significant. This is consistent with analytic theories that predict supersonic sheared flows are needed to stabilize MHD instability. © 2000 American Institute of Physics. [S1070-664X(00)05011-4]

I. INTRODUCTION

It is well recognized that flow shear has a stabilizing effect on magnetohydrodynamic (MHD) and drift-type plasma instabilities.^{1–6} Roughly speaking, the criterion for significant stabilization can be written as^{3,6}

$$\mathbf{k}_\perp \cdot \mathbf{u}'_\perp \Delta x > |\omega|, \quad (1)$$

where \mathbf{u}'_\perp is the velocity shear perpendicular to the magnetic field, \mathbf{B} , \mathbf{k}_\perp is the perpendicular wave number, Δx is the perpendicular extent of the unstable mode, and $|\omega|$ is the absolute value of the mode frequency. For MHD instabilities, $|\omega| \sim c_s/L$ or V_A/L and $k_\perp \Delta x \sim 1$, where c_s is the sound speed, V_A is the Alfvén speed, and L is a macroscopic scale size. Thus, the stabilization condition scales as $|\mathbf{u}'_\perp| \gtrsim (c_s; V_A)/L$. If the flow shear scale is macroscopic, the criterion implies that for maximum flow speeds approaching sonic or Alfvénic speeds, MHD instabilities may be stabilized. This possibility is of great interest for configuring stable magnetic confinement schemes for thermonuclear fusion.^{1,7,8}

In this paper, we investigate whether a Z pinch can be stabilized if the plasma is made to flow along the z axis at supersonic speeds. We employ a nonlinear, three-dimensional numerical MHD simulation for this study. Generally, Z pinches are unstable to sausage (azimuthally symmetric) instabilities as well as kink instabilities. We show that the flow shear suppresses these instabilities. Complete suppression is obtained for high enough sonic Mach numbers (~ 5). For lower Mach numbers, there is a residual wobble of the discharge, confined to the center of the plasma column, that gets smaller as Mach number is increased.

The possibility of stabilizing MHD systems by velocity shear has been proposed recently.^{4,5,7} A discussion of this theoretical background is given in Sec. II. Our numerical model is outlined in Sec. III. In Sec. IV, the equilibrium discharge without flow is set up. In Sec. V, the disruption of

this discharge by instability is described. A momentum source is now turned on to drive flow in the axial direction, u_z . We show, in Sec. VI, that the discharge recovers significantly when the flow shear gets large enough, but a residual wobble of the discharge persists. In Sec. VII, we repeat this numerical experiment for a plasma with an elongated cross section—this is motivated by recent theoretical results that show that elongation is stabilizing.⁹ A fairly complete study is done for an elongation of 4. Some related issues are discussed in Sec. VIII. We conclude in Sec. IX.

The Mach number, M_s , is a key parameter for our study. We define M_s as $M_s \equiv u_z/(T/M)^{1/2}$, where T is the temperature and M is the ion mass. We will define the sound speed as $c_s \equiv (T/M)^{1/2}$.

II. THEORETICAL BACKGROUND

We summarize here theoretical studies on the stabilization of ideal MHD instabilities by velocity shear. The key instabilities are the interchange (sausage) and the kink modes.¹⁰ Theoretical results of the stabilization of these modes from velocity shear are discussed in the following. Since there is a large velocity shear in the system, the Kelvin–Helmholtz instability¹¹ is also discussed.

A. Sausage instability

The sausage instability of a Z pinch is an $m=0$ interchange mode, mediated by the field line curvature. This mode is closely analogous to the Rayleigh–Taylor (RT) instability mediated by a gravitational field. The stabilization of the RT mode was considered in Ref. 4. The RT mode is the ideal MHD interchange of flux tubes resulting in a release of gravitational potential energy if the density gradient is inverted with respect to the gravitational acceleration, g . In the incompressible limit, the growth rate for this mode is $\gamma_g = (g/L_n)^{1/2}$, where L_n is the density gradient scale. In the presence of a velocity shear, V' , the mode is stabilized. Assuming there is no shear in the magnetic field, the stability criterion is given by⁴

$$V' > \gamma_g [\ln R]^{1/2}, \quad (2)$$

^{a)}Permanent address: Department of Physics, University of Maryland, Baltimore County.

where $R \gg 1$ is a Reynolds number based on the RT growth time and the diffusive and viscous time scales. This factor arises because the velocity shear stabilization is primarily a phase mixing process and, so, diffusive processes play an essential, albeit weak, role.

There is a direct analogy between the RT and the $m = 0$ sausage mode in a Z pinch: the replacement $g \rightarrow c_s^2/L_n$ gives the right order of magnitude for purposes of comparison. With this replacement and the assumption that flow profiles have a scale size of the order of the plasma column radius, we may rewrite the above-mentioned stability criterion in terms of the sonic Mach number $M_s \equiv V/c_s$ as

$$M_s > [\ln R]^{1/2}. \quad (3)$$

It can be shown that elongation of the plasma cross section reduces the Mach number requirements.⁹ Basically, elongation reduces the growth rate of the interchange, because the average curvature of the field line is reduced, but does not affect the efficacy of the velocity shear since this is based on the shorter scale of the cross section. As a result, the Mach number requirement goes down as $E^{-1/2}$, where E is the elongation.

B. Kink mode

The effect of velocity shear on the kink mode in a Z pinch was considered analytically by Arber and Howell¹² and Shumlak and Hartmann.⁵ In a Z pinch, the kink mode, typically with $m = 1$, grows on a time scale which is Alfvénic. These authors imposed a z -directed flow and studied the resulting stabilization. Arber and Howell found that the kink mode was stabilized, for certain cases, if the Mach numbers exceeded 2–4. Shumlak and Hartmann considered a Z pinch with a pressure profile that was marginally stable to the $m = 0$ sausage mode (discussed previously). They found a stability criterion given approximately by $V' > 0.1k_z V_A$.

C. Kelvin–Helmholtz instability

Second derivatives in fluid flow can drive Kelvin–Helmholtz instabilities which can have a maximum growth rate that scales as the flow frequency, V' . Wavelengths longer than the velocity shear scale, a , are unstable with the peak growth typically at about $2a$.¹¹ Such an instability would obviate any stabilization tendency of the flow shear on kinks and interchanges. However, the above-given maximum growth rate is quite sensitive to the flow profile. In particular, the growth rate is of order V' only for velocity profiles that include at least one inflexion point (i.e., $V'' = 0$ somewhere). This is the essence of the Rayleigh–inflexion theorem.¹³ If there are no inflexion points, the growth rate drops precipitously, scaling as some fractional power of the inverse of the viscous Reynolds number R . In the numerical experiment we consider here (as well as in fusion applications of interest to us), the laminar flow profile does not have inflexion points.

III. NUMERICAL MODEL

We solve numerically the following set of equations:

$$\frac{\partial n}{\partial t} + \nabla \cdot (n\mathbf{u}) = 0, \quad (4)$$

$$\begin{aligned} \frac{\partial}{\partial t} (nM\mathbf{u}) + \nabla \cdot (nM\mathbf{u}\mathbf{u}) \\ = -T_0 \nabla n - \frac{\nabla B^2}{8\pi} + \frac{\mathbf{B} \cdot \nabla \mathbf{B}}{4\pi} \\ + \nabla \cdot [nM\mu[(\nabla \mathbf{u}) + (\nabla \mathbf{u})^T]] + F_0 \hat{z}, \end{aligned} \quad (5)$$

$$\frac{\partial \mathbf{B}}{\partial t} = -c \nabla \times \mathbf{E}, \quad (6)$$

$$\mathbf{E} + E_0 \hat{z} \equiv -\frac{\mathbf{u} \times \mathbf{B}}{c} + \frac{\eta c}{4\pi} \nabla \times \mathbf{B}. \quad (7)$$

Standard notation is used with M being the ion mass, μ is the viscosity, and η is the resistivity. Isothermal conditions are assumed, for simplicity, with temperature T_0 . An electric field, $E_0(x, y)$, is applied in the \hat{z} direction. F_0 is the z -directed applied force that accelerates the fluid, creating the velocity shear.

The simulation was done in a box of size $1 \times E \times 1$, where E is the elongation in the y direction. For the simulations reported in this paper, we used $E = 1$ and $E = 4$. Hard, conducting wall boundary conditions were used for the boundaries in x and y . Periodic boundary conditions were used in z . No-slip boundary conditions were used for \mathbf{u} at the walls. As mentioned previously, isothermality was assumed and, in addition to the box size being set to unity, we set to unity the sound speed $c_s \equiv (T_0/M)^{1/2}$. Thus, space and time were normalized to the box size and the sound time.

The numerical algorithm is described in detail by Guzdar *et al.*¹⁴ The variables n , \mathbf{u} , and \mathbf{B} are stepped forward in time from some initial condition. The code has been tested in several ways including Alfvén waves, magnetosonic waves, and shock waves. For the spatial resolution used in our study, the condition $\nabla \cdot \mathbf{B} = 0$ is satisfied to less than 1% as defined by the condition $3|\sum_i \partial_i B_i|/|\sum_{i,j} |\partial_i B_j|| < 1\%$. The code also conserves total mass; for the runs reported in the following, total mass was conserved to less than 1%.

IV. EQUILIBRIUM

The axially directed electric field, E_0 , was applied and kept on for the entire simulation. The applied field was taken to be

$$E_0(x, y) = \eta j_0(x, y),$$

$$j_0(x, y) \equiv [1 + 1/E^2](\pi^3/10) \sin(\pi x) \sin(\pi y/E),$$

where η is the resistivity and E is the elongation. For all the runs reported here, unless otherwise stated, we took $\eta c^2/4\pi = 0.002$. We also let the viscosity μ be equal to $\eta c^2/4\pi$. The simulation box was filled with an initial density equal to 1 unit, everywhere, the E_0 field was turned on, and the system was allowed to relax under resistive and viscous

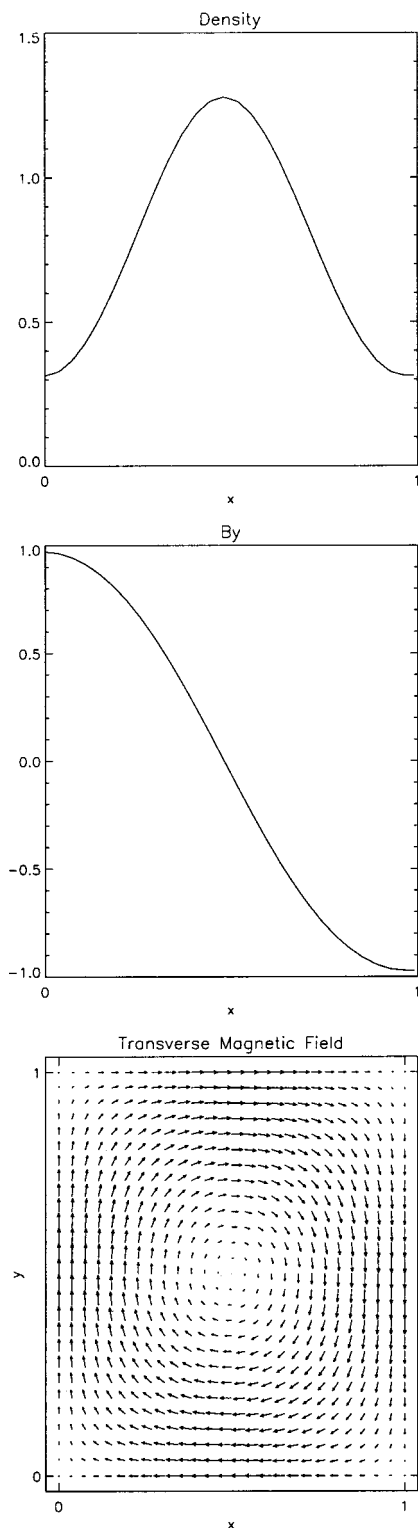


FIG. 1. The equilibrium (laminar) configuration for the square cross section Z pinch. Cuts along the middle for the density and B_y are shown. Also shown is a vector plot of the magnetic field in the perpendicular plane.

dissipation. For $E=1$, the resulting density is shown in the top plot in Fig. 1, which is a cut of the density in x along the y midplane. In the second plot, we show B_y as a function of x in the y midplane. For the electric field picked as above, the maximum value of B_y , for $E=1$, was $\pi^2/10$. The corresponding magnetic field, constituting the equilibrium pinch, is shown in the vector plot.

V. BREAKUP OF DISCHARGE

The “discharge” was initialized as described in Sec. IV. We now added random noise to the density of less than 10^{-3} . After a few sound times, the discharge was seen to go unstable to what appeared to be a combination of $m=0$ and $m=1$ modes. This time sequence is shown in the six grayscale frames in Fig. 2 (total time elapsed is 6 units after random seeding). The grayscale frames are contour plots of a cut, along the y midplane, of the density as a function of x and z . By the last two frames, the density has hit the walls and bounced off of it. Note that the electric field, E_0 , is kept on at all times, tending to drive the axial current. If the simulation is continued further in time, the density is seen to continue to swirl around the chamber in a turbulent manner: There is complete mixing of the density and the current and the discharge never “recovers.” Some of this can be observed in the linear plots in Fig. 2 labeled “Density.” These plots are cuts in density taken along the x axis for $y-z$ midplane; six different cuts are shown, corresponding to the time slices in the grayscale plots. Note the collapse and mixing of the density. Shown also in Fig. 2 is the corresponding time slices for $nu_z(x)$, labeled “Z-Momentum.” The latter values are small indicating that there are no large axial flows forced in the system, yet.

VI. PARTIAL RECOVERY FROM FLOW SHEAR

We now turn on the z -momentum forcing term, F_0 , in Eq. (4). For this simulation, F_0 was taken to be a constant throughout the chamber. Thus, given the no-slip boundary conditions assumed at the walls, the laminar steady state flow profile of u_z would be parabolic. With the turning on of this force, a partial “recovery” of the discharge ensued. This is depicted in Fig. 3. The layout of this set of figures is identical to Fig. 2, the time slices spanning an elapsed time of 15 units. The density is seen to become more localized, in the transverse directions, compared with the turbulent state of affairs in the first frame (or the last frame in Fig. 2). However, the recovery is not to the same level as the first frame of Fig. 2 (i.e., the laminar case), there being a clear and large wobble seen propagating with the average flow speed. The cuts of the density along the midplane clearly show that the density profile has hardly reverted to its laminar shape, in fact it is almost flat. From the $nu_z(x)$ cuts, we note that the maximum Mach number for this run is about 0.5 (the Mach number measured is less than the corresponding laminar Mach number for the force applied, a result of the turbulence—the latter was 1.5).

We next increased the applied force to attain higher Mach numbers. The wobble decreased but remained substantial. This is summarized in Fig. 4: The cut of $nu_z(x)$ shows that the flow speed increases to a maximum of about Mach 1.5. The corresponding state of the discharge, taken at the maximum Mach number, is shown in the grayscale plot of the density. The linear cut of the density is also shown and indicates that the density profile, while recovering at the flanks, is hardly close to the laminar profile. At this level of Mach number, the wobble was noticed to be a “frozen in” structure propagating at some average speed along the direc-

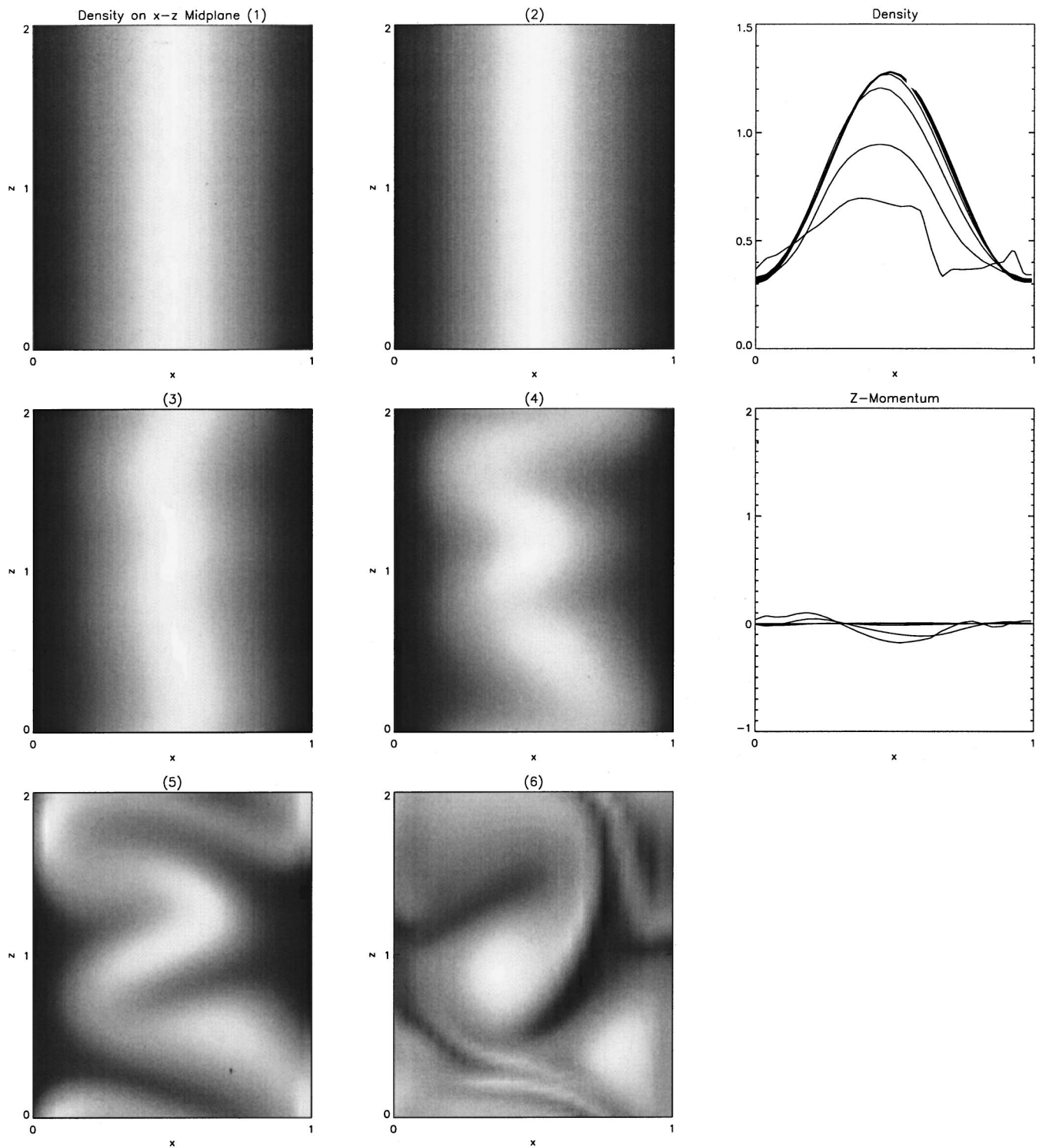


FIG. 2. The breakup of the square cross section discharge from sausage and kink instabilities. The grayscale plots are slices along the middle of the density contours. Six consecutive time frames are shown. Total time elapsed is six sound times. Also shown are cuts in density and axial flow Mach number, six time frames overlaid. Note the density collapse and that there is no average axial flow.

tion of the flow. This can be seen in the grayscale plots of Fig. 5. The latter are snapshots of the discharge viewed end-on, i.e., they are cuts in the $x-y$ plane. The azimuthal rotation of the wobble is clearly evident.

VII. ELONGATED CROSS SECTIONS AND RECOVERY

At this point in the numerical experiment, we took into consideration the results of a theoretical calculation that

showed that elongated plasma configurations would be easier to stabilize by velocity shear than square/circular cross sections.⁹ The theory indicated that the Mach number requirements for stabilization would go down as $E^{-1/2}$, where E is the elongation. We thus reconfigured the numerical experiment to study plasma elongation of $E=4$. A similar sequence as in Sec. VI was done. The $E=4$ study was done more systematically, through a much wider range of Mach

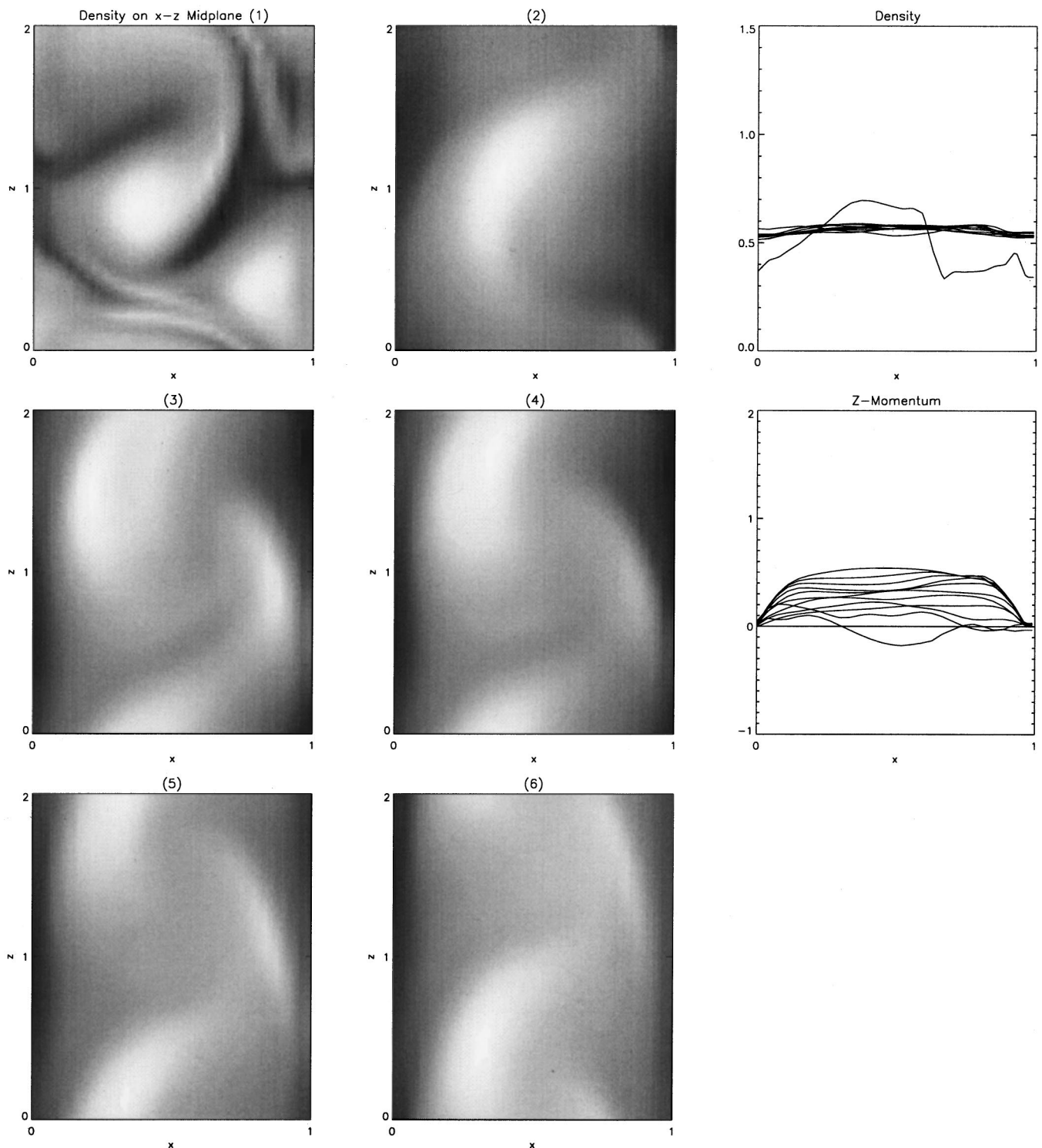


FIG. 3. The beginnings of the recovery of the discharge as axial flow comes up (time elapsed=9 sound times after onset of axial forcing of flow). Same layout as in Fig. 2. Plasma has been pulled away somewhat from the walls with a wobbly but otherwise relatively quiescent density column evident. The density cuts, however, show suppression in turbulence but an essentially flat density. The Mach number has built up to a maximum of about 0.5.

numbers (M_s ranged from 0 to 6). In this series of runs, we achieved almost complete stabilization of the pinch, i.e., the wobble was reduced to less than 5%. The results are summarized in the following figures.

Figure 6 contains linear cuts of density along the midplane in the x direction, taken for different measured Mach numbers. In each case, the applied force was increased and

the system was allowed to reach a wobbly steady state before the density cut was taken. The first frame is a reference case where we show the laminar density cut, i.e., the case when there is no variation allowed in the z direction. In the remaining five frames, we show density cuts, in the wobbly steady state, for peak Mach numbers of approximately 0.3, 1.4, 2.2, 3.7, and 4.8. The laminar profile (dashed) is overlaid in each

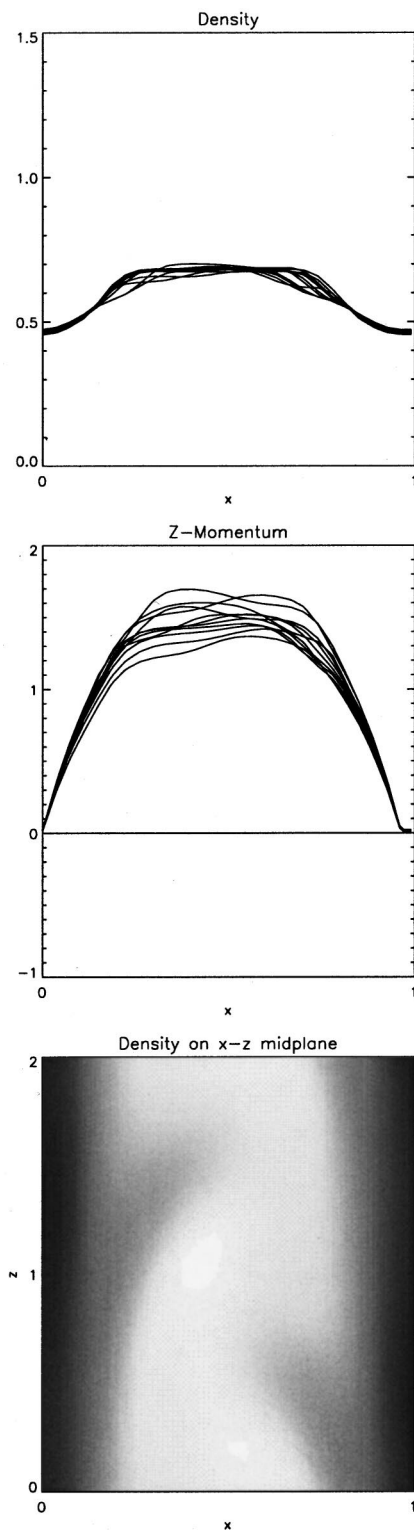


FIG. 4. The discharge at higher Mach number. The maximum Mach number is about 1.5 and the density cuts show a partial recovery but with an extended flattop. The grayscale plot exhibits the wobble.

case. The progression shows clearly that the density approaches the laminar limit as the Mach number increases. In particular, it is clearly seen that the stabilization proceeds from the flanks and grows inward toward the core. This phenomenon is consistent with the idea that the velocity shear, being parabolic in the laminar limit, should be maximum at

the flanks and go to zero at the core: As the maximum Mach number increases, the stabilization should penetrate deeper into the core. In Fig. 7, we show the flow profile snapshots overlaid for the corresponding Mach numbers. The corresponding grayscale contour plots of the density are shown in Fig. 8. Note the clear reduction in the wobble radius as we increase the Mach number.

To assess the above-mentioned progression to laminarity in more quantitative terms, we defined the function

$$W(x,y,z) = |1 - n(x,y,z)/n_0(x,y)|, \quad (8)$$

where $n_0(x,y)$ is the density in the laminar limit. This function quantifies how close we are to attaining laminarity. In Fig. 9, we plot \bar{W} versus the Mach number for the numerical experiment of $E=4$. Here \bar{W} is the value of W averaged over the entire volume. The standard deviation is shown in the error bars, reflecting the amplitude of the wobble. Figure 9 shows that deviations from laminarity are reduced to less than 5% at the highest Mach numbers. In this way, we can quantify the level of stabilization achieved by velocity shear.

The overall significance of the wobble needs to be assessed. Clearly, the discharge has been stabilized as far as gross MHD instability is concerned: The discharge has integrity and the plasma is contained inside of a radius that is very close to the laminar radius. One might even argue that the wobble is irrelevant in that the plasma as a whole is confined. From the viewpoint of confinement of plasma for thermonuclear fusion, we believe that the real significance of the wobble is not in terms of gross MHD stability but, rather, the transport that the wobble would cause. Clearly, the transport in the core where the wobble is noticeable would be quite large. It is also possible that the transport in the flanks may be significant on account of the fact that the residual wobble, while quite small for gross motions, might nonetheless give significant transport. A complete assessment of the transport is outside the scope of the paper. However, it is useful to quantify to some extent the spatial distribution of the wobble. To this end, we show in Fig. 10 a plot that achieves this by quantifying the value of an appropriate average of W as a function of radius across the minor cross section of the discharge (this plot was done for the highest Mach number of 4.8). To obtain this plot, we averaged $W(x,y,z)$ over all z and over an annular rectangular area, centered about some reference rectangle and of width equal to three grid points. In Fig. 10, we plot this value of W versus the distance of the annulus from the outer wall on the x axis. Figure 10 clearly indicates that the deviations from laminarity increase as we go inward to the core.

Our results show clearly that we have achieved >95% stabilization from velocity shear and that the residual wobble is concentrated mainly in a small radius about the core. However, fairly substantial Mach numbers are needed. In addition, transport from the wobble remains to be assessed. Future work must address how much toroidal magnetic field might be needed to suppress the residual wobble.

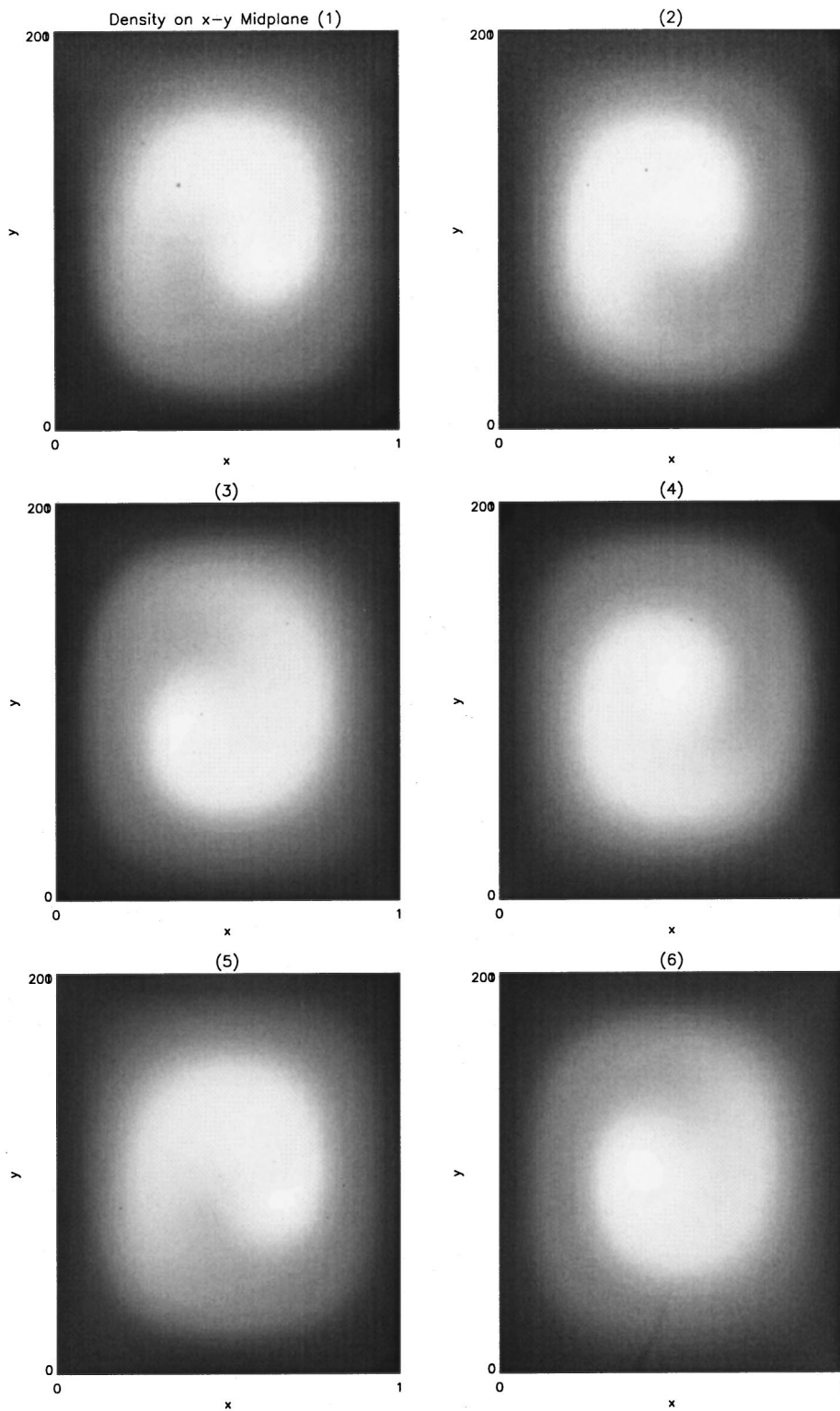


FIG. 5. End on view (x - y plane) of the density contours corresponding to the 1.5 Mach number discharge of Fig. 4. Note the rotation of the wobble. The data indicated an almost frozen-in translation of the wobble along the axis.

VIII. OTHER ISSUES

A. Hysteresis

One possible mitigating factor in the above-obtained understanding is hysteresis in the level of wobble as a function of the applied force. To test for this, we first set up a laminar equilibrium with flow, obtained numerically by not seeding the equilibrium with any noise with z variations, and then

adding z noise once a steady state laminar flow had been obtained. This test was done for the data point in Fig. 9 corresponding to the Mach number of 2.2. If there were any hysteresis, the instability and wobble resulting from this procedure would have a character different from that reported for the corresponding data point mentioned previously. This was found not to be the case. We concluded therefore that there was no hysteresis.

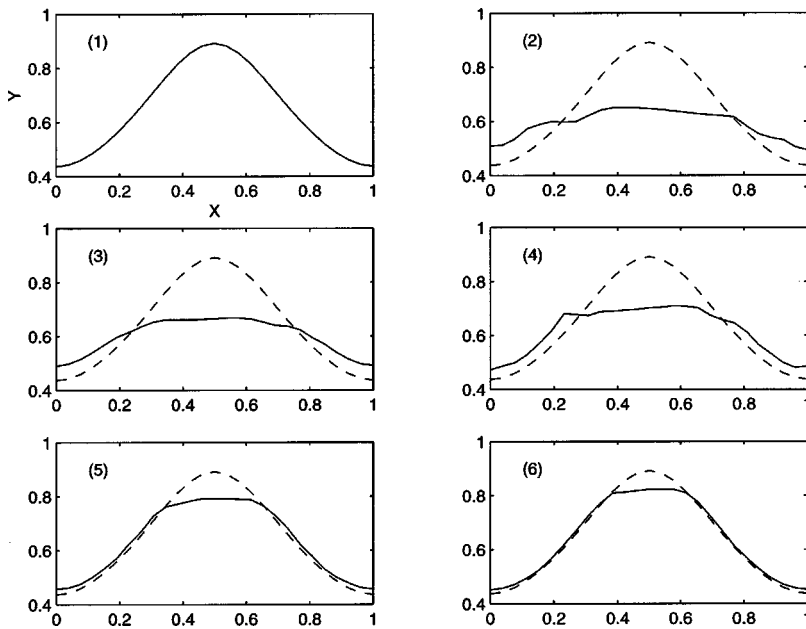


FIG. 6. Data for elongation=4 and higher Mach numbers. The top left frame is the laminar density, shown for reference. The remaining five density slices correspond to increasing Mach number, with the laminar density overlaid (dashed). Approach to laminarity is clearly evident. Each cut was taken after the discharge had relaxed to a turbulent steady state. The corresponding Mach number slices are shown in Fig. 7. The corresponding maximum Mach numbers are 0.3, 1.4, 2.2, 3.7, and 4.8.

B. Dependence on Reynolds number, R

The stability criterion for interchange modes as given by Eq. (2) predicts a dependence on the Reynolds number, R . As given in Ref. 4, the Reynolds number is proportional to the sound speed and inversely proportional to the square root of the product of the viscosity and the resistivity. We tested our results for sensitivity to R as predicted by (2) and found qualitative agreement as follows. In the middle of a wobbling discharge that had reached some steady conditions, we increased the viscosity and resistivity each from 0.002 to 0.005, at the same time increasing the applied force F_0 and electric field by the same factor. Thus, we would not expect there to be any change in the laminar flow speed. We now waited for the discharge to settle and then observed the new

steady state. We found that the wobble was reduced. As one measure, the peak density went from 0.67 to 0.77. This trend is qualitatively consistent with that predicted from criterion (2).

C. Dependence on elongation, E

For a given Mach number, we expect the wobble to increase if the elongation E were reduced. This expectation arises from the analytical result, discussed previously, that the Mach number requirement goes down as $E^{-1/2}$. This was qualitatively confirmed as shown in data taken at $E=1$ in Figs. 11 and 12. In Fig. 11, we show a cut of the flow velocity u_z vs x for $E=1$. This is to be compared with the

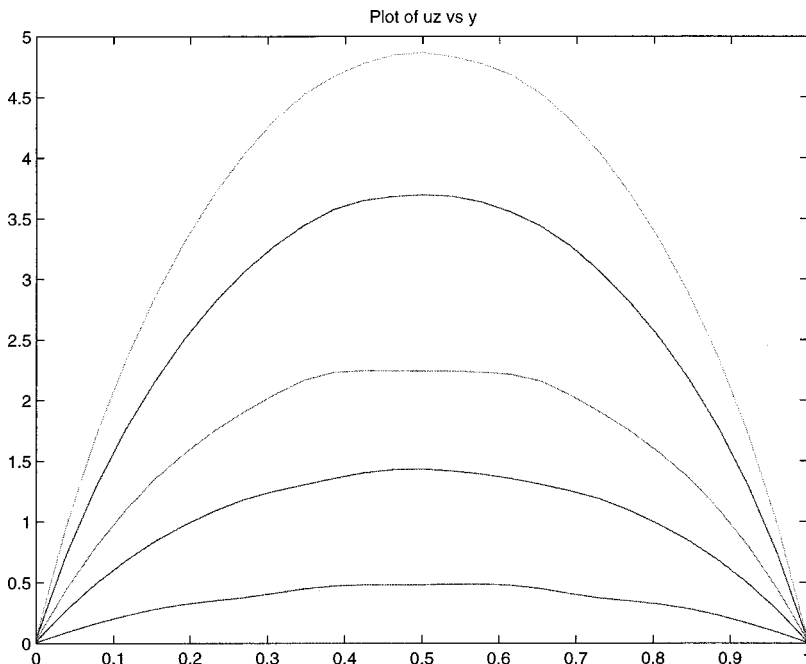


FIG. 7. Mach number slices, overlaid for five different forcing terms. Each slice corresponds to the density slices in Fig. 6. Note the flow is practically parabolic at the high speeds, evidencing an almost laminar discharge.

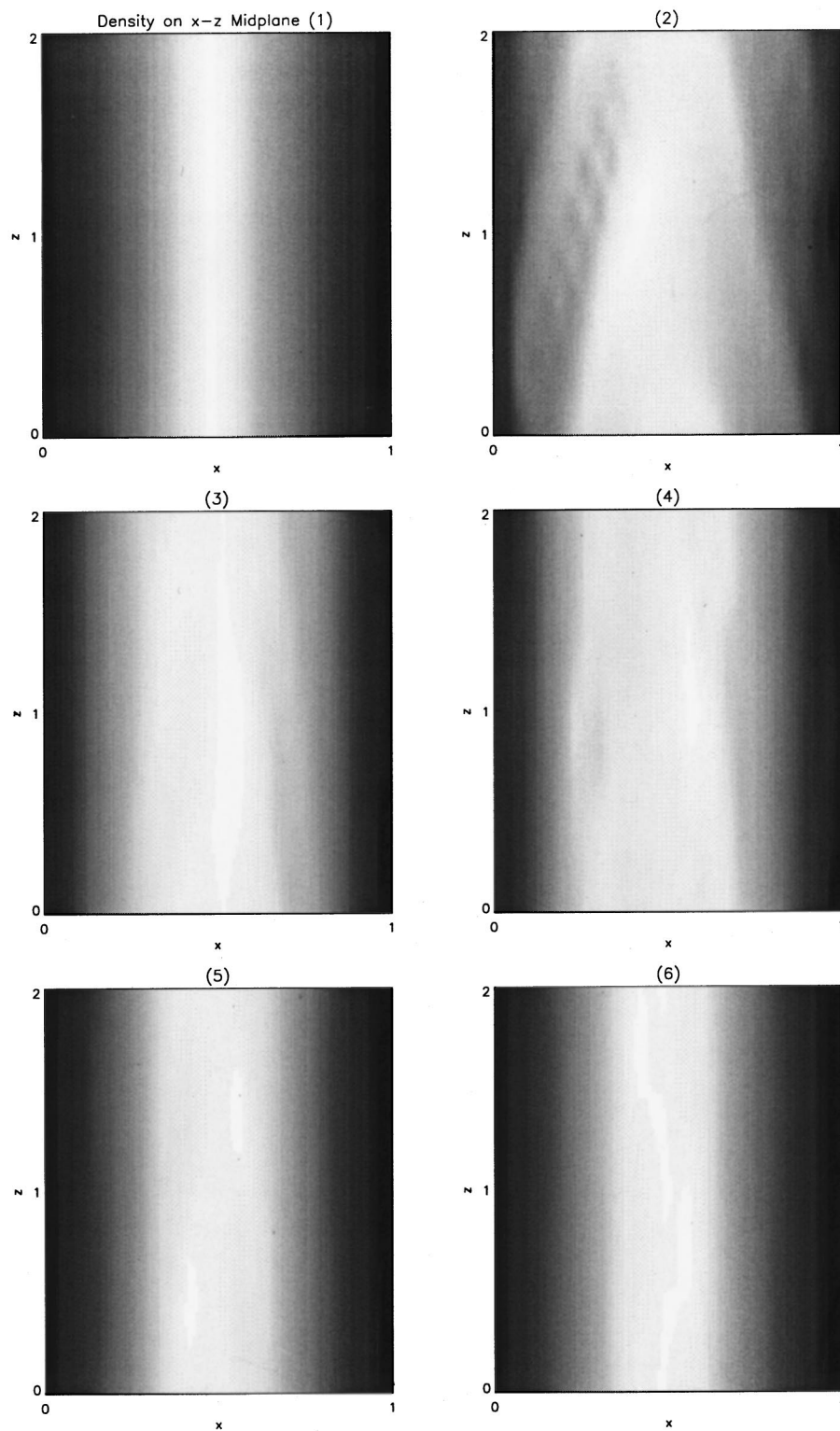


FIG. 8. Contour slices of the density corresponding to the six plots in Fig. 6.

corresponding cut taken for $E=4$ in Fig. 7: For commensurate Mach numbers, the $E=4$ cuts show much more laminarity, in fact they are almost parabolic, compared with those of $E=1$. In Fig. 12, we show the density cut that goes with the u_z cut of Fig. 11. This should be compared with the corresponding $E=4$ density cuts of Fig. 6—the latter are clearly more laminar for the same Mach number.

D. Kelvin-Helmholtz

Our numerical experiment was run for an axial length of 1 unit. We chose this because the most strongly unstable modes, linearly and nonlinearly, were found to have a wavelength that was shorter than one unit, as is evident in the grayscale plots of Fig. 2. This choice, however, precludes

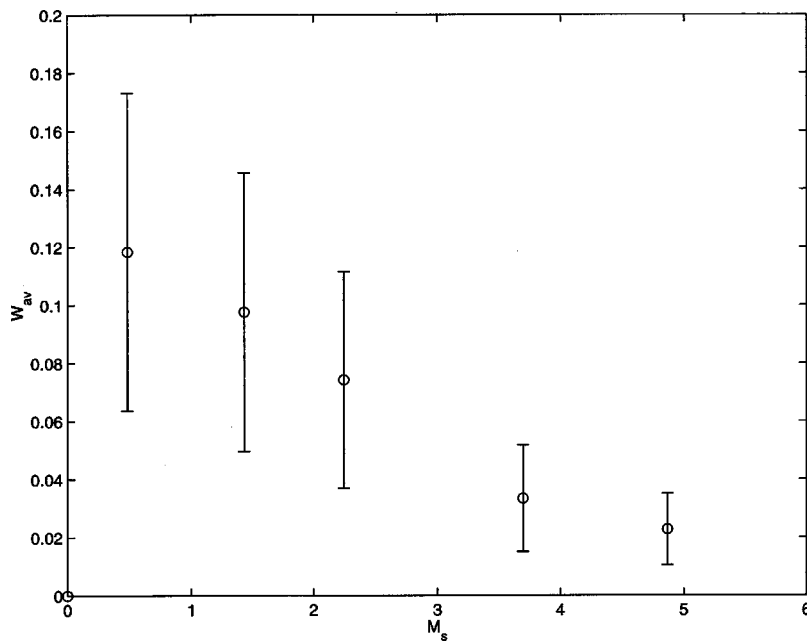


FIG. 9. Measure of approach to laminarity with increasing Mach number. The abscissa is the maximum Mach number. The ordinate is the W function, as defined in the text, averaged over the volume. W measures the deviation of the density profile from laminarity.

any turbulence from wavelengths greater than 1 unit, where one expects Kelvin–Helmholtz (KH) instability. Analytic theory predicts that the KH should be fairly weakly unstable, in accordance with the Rayleigh–inflexion theorem.¹³ We have not yet checked how a weak KH would affect the residual wobble, if at all. One difficulty is that, given the weak growth of the KH and that the mode structure has boundary layer localizations, one would have to run at higher resolution.

E. Conservation of mass

For the data taken in this numerical experiment, the volume-integrated density was monitored to check conservation of total mass. In all cases, we ensured that total mass was conserved to less than 1%. We present here the results of

the mass conservation tests for the data reported in Figs. 6 and 12. For the six time slices of Fig. 6 as shown, we compare the volume-integrated density at times 3, 4, 5, 6 to that at time 2. The deviations $[1 - \langle n \rangle / \langle n_2 \rangle]$ are 0.0019, 0.0042, 0.0067, 0.0081, where $\langle n \rangle$ is the volume-integrated density at a given time and $\langle n_2 \rangle$ is the one at time 2. The deviation $[1 - \langle n_1 \rangle / \langle n_2 \rangle]$, n_1 being the laminar initial condition, is -0.019 . This is higher and of the opposite sign because, between the two time slices, random noise in the density at roughly the 1% level was inserted to “seed” the instability. Also, conserved quantities are violated more severely in the early, more violent instability event. Finally, for the data shown in Fig. 12, the deviation, as defined previously, between the two curves shown is -0.0030 .

The notion that there is approximate conservation of

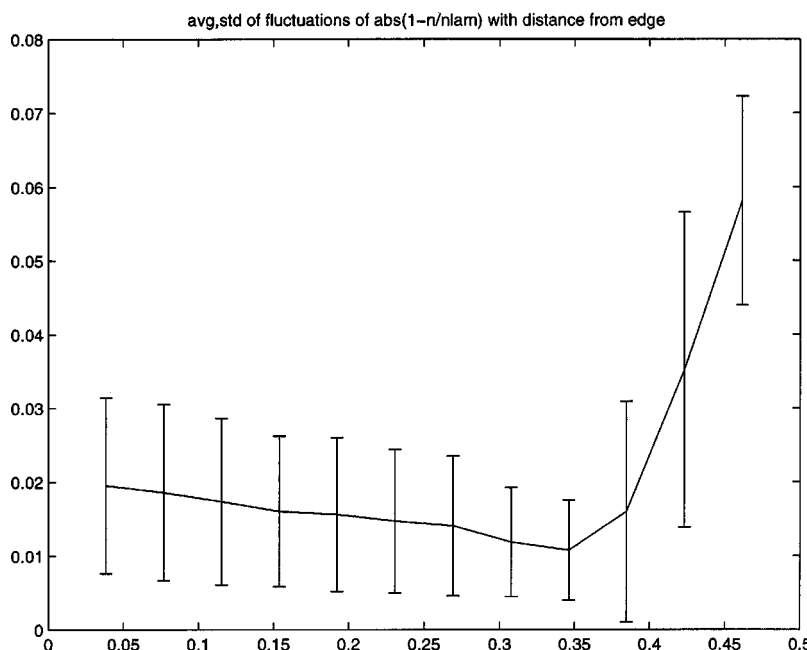


FIG. 10. Measure showing that deviation from laminarity is largest near the central axis. The W function, averaged over z and over a box annulus in the x – y plane, is plotted vs distance of annulus from the outer wall on the x axis. The wobble maximizes near the axis.

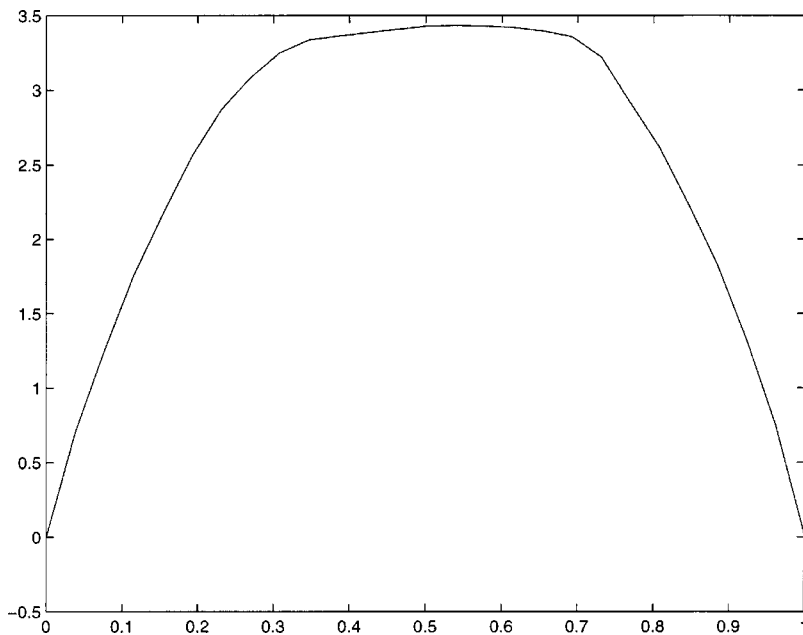


FIG. 11. A Mach number slice for elongation=1, to be compared with Mach number slices for elongation=4 shown in Fig. 7. Note that for the same peak Mach number, the elongation=1 profile has a much larger flattop.

mass can also be formulated by eyeballing a figure such as Fig. 6. At first glance, the plots give the appearance that there is a larger mass loss in the center compared to the flanks. However, there is more volume at larger radii, volume going as radius squared in this cylindrical case, which makes up for the apparent small rise in density in the flanks. In addition, we note that Fig. 6 is only a single slice in z : different slices in z would show somewhat different profiles since there are wobbles in z ; thus, a single slice may be misleading.

IX. DISCUSSION

We have asked the question whether externally forced velocity shear can stabilize the kink and sausage instabilities of a Z pinch. We found the following.

(1) Velocity shear indeed stabilizes the Z pinch. However, the stabilization is manifested as a gradual approach to laminarity with increasing Mach number of the flow. At a given Mach number, there is a residual wobble that is localized to the core where the velocity shear is weak (for a parabolic laminar flow profile). The wobble goes down with increasing Mach numbers, with the flow profiles reaching laminar conditions in about 98% of the volume for a Mach number of about 5.

(2) The wobble is benign in the gross MHD sense in that the discharge plasma is contained almost within the “laminar” radius. Thus, in this sense, the MHD stabilization of the Z pinch is complete. However, the transport from the wobble needs to be assessed. A “marginal stability” theory for the transport is indicated.

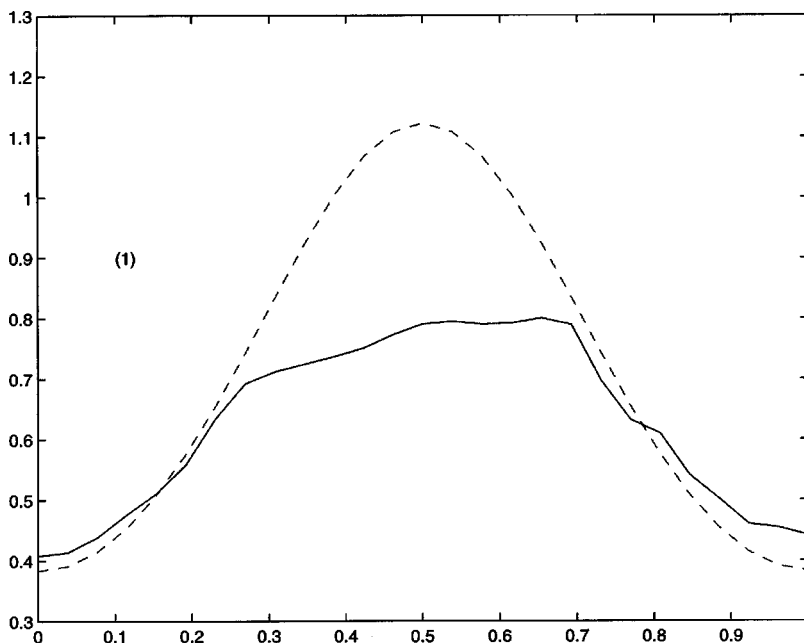


FIG. 12. Density slice corresponding to the Mach number slice of Fig. 11 (elongation=1). Compare this with the slices in Fig. 6 for commensurate Mach number.

(3) It is quite likely that the addition of a relatively weak axial magnetic field in the equilibrium would suppress the wobble from magnetic shear stabilization, *à la* the Suydam criterion.¹⁰ Since the wobble is relatively weak, the requisite toroidal field may be small. This would be a desirable outcome. We have not attempted to resolve this issue systematically in this work. As a minimum test, we have found that a B_z of about 1 unit, i.e., of the order of the maximum azimuthal field, stabilizes the pinch completely as expected.

(4) For a given turbulent Mach number, elongation of the plasma cross section helps to reduce the wobble. Theoretically, this effect is expected to scale as $E^{-1/2}$. We have qualitatively confirmed this trend.

(5) The Z pinch has both kink and interchange modes. It is not possible to separate in this study which mode is more important. One way to do this would be to insert an internal axial current carrying conductor in this simulation, run at low β , and turn off E_0 so that the field is almost the vacuum field with no kinks possible. A numerical experiment then would settle whenever the wobble is a result of the interchange. Earlier work seems to suggest that it is the interchange that is causing the wobble.

A numerical simulation run by Shumlak¹⁵ on this problem suggests a stronger stabilization from velocity shear. His data do not seem to have a wobble in the flow-shear stabilized state. The requisite Mach numbers are somewhat lower. There is one important difference between the two numerical experiments that could explain the discrepancy. In our case, the flow is forced externally by a constant force; with no-slip boundary conditions, this would set up a parabolic laminar flow profile. In the case of Shumlak, the laminar flow profile is numerically held steady and, further, it is chosen to be linear in radius, zero at the origin and a nonzero value at the radial boundary. Thus, nowhere in the radius does Shumlak's

simulation have a vanishing first derivative of the flow. Our wobble is restricted to the center of the column, where the du_z/dr is small. We conclude that it is the first derivative of the flow that does the stabilizing.

For the recently revived fusion scheme of centrifugally confined plasma,^{16,7} the above-mentioned results indicate that an axial (toroidal) magnetic field may be necessary to create a good confinement device using velocity shear stabilization. In an optimistic scenario, the required toroidal field might be quite weak.

ACKNOWLEDGMENTS

We acknowledge useful conversations with Dr. R. J. Goldston and assistance with the data analysis from Bryan R. Osborn. This work was supported by the Department of Energy.

¹R. Groebner, Phys. Fluids B **5**, 2343 (1993).

²H. Biglari, P. H. Diamond, and P. W. Terry, Phys. Fluids B **2**, 1 (1990).

³A. B. Hassam, Comments Plasma Phys. Control. Fusion **18**, 275 (1991).

⁴A. B. Hassam, Phys. Fluids B **4**, 485 (1992).

⁵U. Shumlak and R. Hartmann, Phys. Rev. Lett. **18**, 3285 (1995).

⁶R. E. Waltz, R. L. Dewar, and X. Garbet, Phys. Plasmas **5**, 1784 (1998).

⁷A. B. Hassam, Comments Plasma Phys. Control. Fusion **18**, 275 (1997).

⁸M. W. Kissick, J.-N. Leboeuf, S. C. Cowley *et al.*, Phys. Plasmas **6**, 4722 (1999).

⁹A. B. Hassam, Phys. Plasmas **6**, 3772 (1999).

¹⁰J. P. Freidberg, *Ideal Magnetohydrodynamics* (Plenum, New York, 1987).

¹¹S. Chandrasekhar, *Hydrodynamic and Hydromagnetic Stability* (Oxford University Press, Oxford, 1961).

¹²T. D. Arber and D. F. Howell, Phys. Plasmas **3**, 554 (1996).

¹³C. C. Lin, *The Theory of Hydrodynamic Stability* (Cambridge University Press, Cambridge, 1996).

¹⁴P. N. Guzdar, J. F. Drake, D. R. McCarthy, A. B. Hassam, and C. S. Liu, Phys. Fluids B **5**, 3712 (1993).

¹⁵U. Shumlak (private communication).

¹⁶B. Lehnert, Nucl. Fusion **11**, 485 (1971).